Bulletin of the Seismological Society of America, Vol. 95, No. 5, pp. 1637–1653, October 2005, doi: 10.1785/0120040158

The Effect of Elastic Layering on Inversions of GPS Data for Coseismic Slip and Resulting Stress Changes: Strike-Slip Earthquakes

by Elizabeth H. Hearn and Roland Bürgmann

Abstract We investigate the effect of depth-dependent elasticity on slip inversions and coseismic stress change estimates for large strike-slip earthquakes, using a series of hypothetical models and the 1999 Izmit, Turkey earthquake as examples. Slip inversions are performed using both semianalytical and finite-element solutions for surface displacements due to a shear dislocation in layered and uniform elastic Earth models. We find that incorporating realistic increases to shear modulus (μ) with depth in our inversions increases recovered centroid depth and seismic potency relative to uniform elastic half-space models. Recovered seismic moment is up to 40% greater for models incorporating depth-dependent μ than it is for uniform elastic half-space models. Incorporating depth-dependent μ also increases our estimate of the maximum slip depth for the Izmit, Turkey, earthquake (to at least 20 km). Our estimates of coseismic stress change in the upper crust do not change significantly when we incorporate depth-dependent elasticity in our inversions, as long as slip at depth is tuned (increased) to match surface displacements. Coseismic differential stresses in the lower crust increase by up to a factor of 3 in the near field, but further from the fault, stresses from layered and uniform elastic models are approximately equal. With increasing depth in the mantle, the ratio of modeled differential stresses for the layered and uniform elastic models approaches the ratio of mantle μ values for these two models. We conclude that models of postseismic viscoelastic relaxation following large strike-slip earthquakes should incorporate depth-dependent elasticity, but that uniform elastic half-space models are adequate to calculate coseismic Coulomb stresses in the upper crust for most triggering studies.

Introduction

Space-geodetic techniques for measuring surface deformation have advanced to the point where detailed patterns of coseismic surface deformation are routinely characterized for large earthquakes. These advances (particularly for GPS and InSAR) have led to increasingly detailed inversions of coseismic displacements for slip on rupture surfaces. Inversions of surface displacements for slip frequently rely on analytical solutions for deformation due to dislocations in an elastically uniform half-space (e.g., Chinnery, 1961; Okada, 1985). Although analytical and semianalytical solutions exist for deformation due to a dislocation in an elastically layered half-space (see summaries by Wang *et al.*, 2003 and Zhao *et al.*, 2004), these solutions are not usually used in inversions of geodetic displacement data for slip (there are exceptions, e.g., Simons *et al.* [2002] and Fialko [2004]). However, when the Earth's layered elastic structure is ignored, seismic potency and centroid depth may be underestimated for earthquakes occurring in the uppermost, low-μ layer (e.g., Rybicki, 1971; Savage, 1987, 1998; Pollitz, 1996). If the elastic half-space is modeled with a shear modulus (μ) of about of 30 GPa, which is typical for upper crustal rocks, seismic moment (i.e., seismic potency times μ) and coseismic stress changes are underestimated as well. We have demonstrated that surface deformation from the 1999 Izmit earthquake can be modeled to within error tolerances by both a M_o 1.7 $\times$ 10^{20} Nm (M_w 7.4) earthquake in an elastically uniform Earth (with μ = 30 GPa) and a M_o 2.5 $\times$ 10^{20} Nm (M_w 7.5) earthquake in a layered elastic Earth (Hearn *et al.*, 2002). Since an understanding of slip patterns is important to studies of earthquake dynamics, the potential for such large errors in slip inversions based on widely used uniform elastic half-space models could pose a serious problem if the Izmit result is typical for large, strike-slip earthquakes. To investigate how the layered elastic structure of the Earth affects inversions of GPS site displacements for coseismic slip (and hence estimates of coseismic stress change), we calculate deformation due to three hypothetical strike-slip earthquakes in a variety of layered elastic Earth models. We also present detailed slip inversions for the 1999 Izmit, Turkey, earthquake, incorporating 1D elastic

structure, and describe how and why results of these inversions differ from Okada (1985) slip inversions.

Methods

We compute models of an earthquake rupture using linear least-squares inversion methods to find a slip distribution that minimizes misfit to measured coseismic displacements weighted by measurement errors (i.e., the weighted residual sum of squares, or WRSS) while preserving smoothness of the slip distribution (e.g., Du *et al.*, 1992; Bürgmann *et al.*, 2002). We use the bounded variable least-squares (BVLS) method (Stark and Parker, 1995) to impose nonnegativity (that is, right-lateral slip only) on the estimated slip values (Price and Bürgmann, 2002). A finite-difference approximation of the Laplacian represents the roughness of the estimated slip distribution (Harris and Segall, 1987; Du *et al.*, 1992), and the sum of this roughness (scaled by the smoothing parameter β) and the WRSS is minimized in the inversion. Hence, the extent to which smoothness is enforced at the expense of fit to surface displacements is controlled by varying β. We use a Tikhonov plot to select an optimal value of β, that is, a value that suppresses spurious structure in the slip distribution while not smoothing out salient features. The inversion requires as input a data kernel **G**. **G** is a matrix of Green's functions, which relate slip on individual fault patches to surface deformation at all surface observation points. **G** is usually calculated using the Okada (1985) analytical solution, in which the Earth is assumed to be an elastically uniform half-space. (From now on, we will refer to this as the Okada method, and to slip models based on the Okada method as Okada models.) We employ two additional techniques to calculate **G** for a transversely isotropic elastic model. In all of our models, we assume that the Poisson's ratio (ν) is 0.25, so the only Lamé parameter varied for each model layer is μ.

Semianalytical Approach

The first method is a semianalytical solution (Wang *et al.*, 2003), which uses a modified (orthonormalized) propagator algorithm to generate Green's functions at equally spaced points (EDGRN), and a convolution routine (EDCMP) to calculate Green's functions for displacements at user-supplied points (e.g., GPS site coordinates). The FORTRAN code for EDGRN and EDCMP is available online via the Computers and Geosciences web page (www.iamg.org/CGEditor/index.htm). These codes are used to generate Green's functions for slip on all fault patches for a particular rupture, which are then assembled to form **G**. In this article, we will refer to the Wang *et al.* (2003) method as the WEA method, and models based on the WEA method will be called WEA models.

Finite-Element Approach

The second technique for generating **G** involves using a finite-element (FE) code (GAEA, Saucier and Humphreys, [1993]) to forward-model surface displacements resulting from slip on individual fault patches (using split nodes; see Melosh and Raefsky, [1981]). The finite-element mesh used to generate the individual Green's functions covers a region of 1200 km by 700 km, and is 250 km deep (Fig. 1). Elements are 2 km on a side around the slipping patch, and increase in size with distance. Taking advantage of the symmetry of the problem, the mesh covers half of the region surrounding the slipping patch. Along the side boundary that bisects the slipping patch, nodes are permitted to displace only horizontally and parallel to the slip direction. All other model boundaries (except the free top surface) are fixed (Fig. 1). Since uniform slip on square patches cannot be represented properly with either linear or quadratic finite-element shape functions (due to the sharp slip-patch edges), ramp functions with slip linearly decreasing from a central nodal high are modeled. The integrated moment for this ramp function is scaled to match that of a 4-km-square patch, slipping 1 m.

Because we assume that elasticity varies only with depth, only one elastic FE model is required for each patch depth. To generate the Green's functions for each fault patch along the rupture surface at a particular depth, we first calculate the GPS site coordinates relative to the center of the patch, and then use the nodal displacements and element shape functions to calculate displacements at these coordinates.

Our approach differs from that of Hearn *et al.* (2002), in which a single FE model represents the entire earthquake rupture. In the Hearn *et al.* (2002) model, the smallest model elements along the fault were 5–10 km wide (nodal spacing of 2.5 km or more), and 6 km in vertical dimension. In this study, the effective element dimension along the rupture is a uniform 2 km (nodal spacing of 1 km). Also, Hearn *et al.* (2002) used a Monte Carlo approach to solve for coseismic slip, rather than a more formal BVLS inversion technique, and were unable to distinguish between models with different lateral distributions of slip (but similar seismic potency) below about 12 km. Zhao *et al.* (2004) use finite elements to explore the effect of layered elasticity on coseismic deformation, but they do not investigate the effect of layered elasticity on inversions of displacement data for coseismic slip.

Modeled Earthquakes

Hypothetical Strike-Slip Earthquakes

We examine how elastic layering influences slip inversions by (1) forward-modeling surface displacements due to slip in a layered elastic model, and then (2) inverting these displacements, assuming an elastically uniform model. We model strike-slip earthquakes with 3 m of slip on ruptures with dimensions of 32 × 16, 64 × 16, and 64 × 24 km. Moment magnitudes for these earthquakes would range from 7.1 to 7.5. (Typical slip for an earthquake with a 32-km

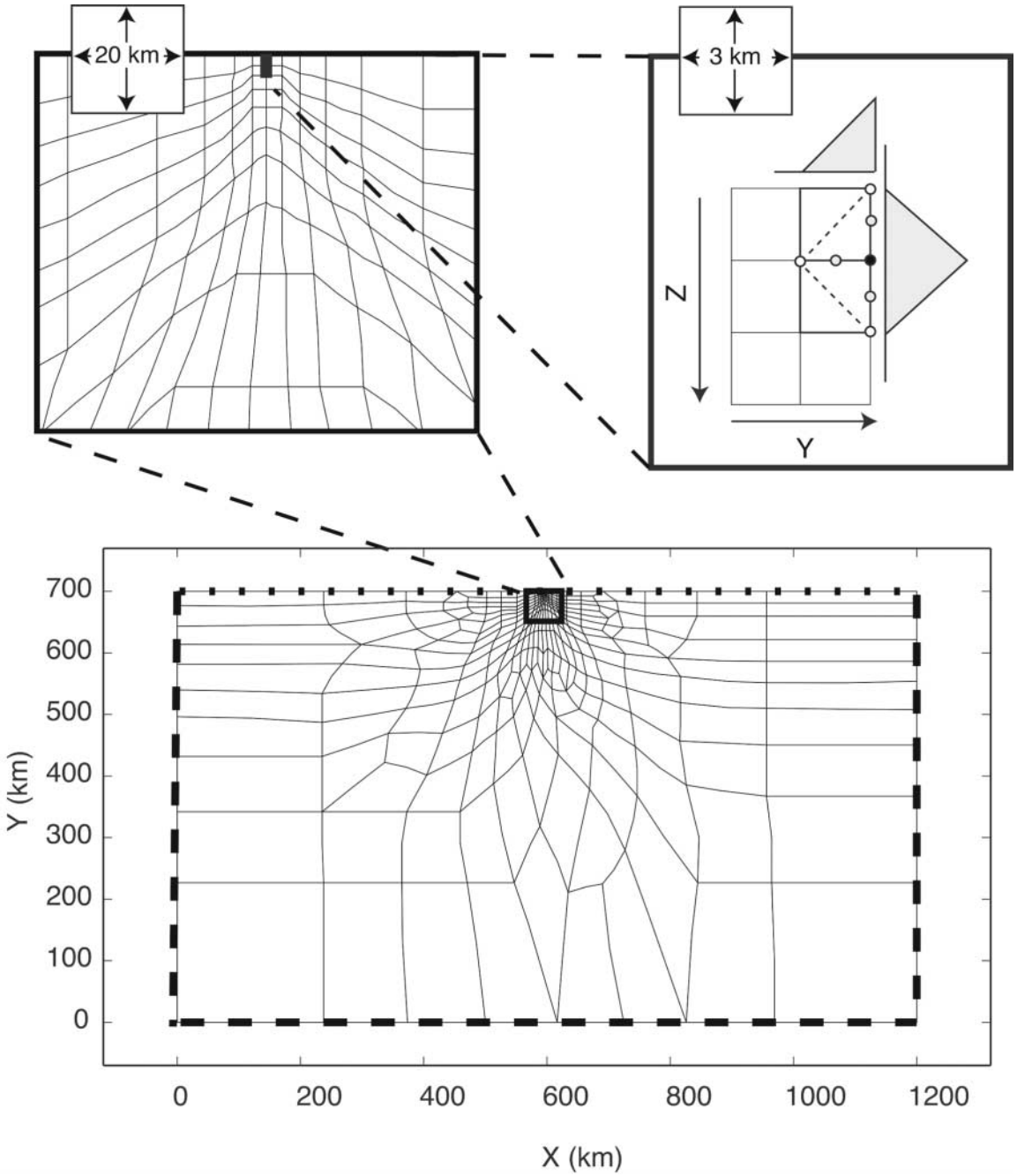

Figure 1. Finite-element mesh used to generate Green's functions: (a) mesh showing boundaries; (b) zoomed-in view; and (c) view of the modeled dislocation (split nodes). Since the problem is symmetric, the mesh covers one half of the slip patch and surrounding region. Along the bisecting boundary, only fault-parallel slip is permitted (dotted line). The other three side boundaries and the bottom boundaries are fixed (dashed lines). Since square dislocations with uniform slip and sharp edges cannot be represented by the FEM, diamond-shaped patches were used and slip was tapered linearly from a central maximum to the edges. Slip integrated over area (potency) was set equal to potency for unit slip on the Okada model tiles (4 km by 4 km).

rupture length is much less than 3 m [Wells and Coppersmith, 1994], but since this is a linear problem, assuming a slip of 3 m does not affect the results significantly, other than scaling them by a factor of 3.) In addition to a uniform-elasticity model with shear modulus (μ) = 30 GPa, we examine four models with layered elastic structure (Fig. 2). The models comprise three layers corresponding to upper crust, lower crust, and mantle, respectively, at depth intervals of 0–16, 16–32, and 32+ km. In each case, values of μ for the top and bottom layers are 30 and 60 GPa. For the intermediate (lower crust) layer, μ is 30, 40, 50, or 60 GPa for elastic models LAY1 through LAY4. Displacements are calculated at hypothetical GPS sites spaced at 15-km intervals within about 90 km of the modeled rupture (i.e., within 1.5 to 3 times the modeled rupture length; see Fig. 3a). In the slip inversions, 1σ measurement errors of 2 and 10 mm, respectively, are assigned to the forward-modeled horizontal and vertical displacement components. GPS data from recent large earthquakes support our assumption of approximately equal north and east displacement errors and a negligible covariance between these errors (e.g., Reilinger *et al.*, 2000; R. King, personal comm., 2002).

1999 Izmit, Turkey, Earthquake

The Izmit rupture is represented using the smooth fault geometry of Feigl *et al.* (2002), which is a 156-km-long surface extended to a depth of 32 km and discretized into 312 approximately 4-km-square patches. The elastic structure for the Marmara region lithosphere has been estimated by teleseismic, strong motion, and active source seismic studies (Bouchon *et al.*, 2002; Karahan *et al.*, 2001; Karabulut *et al.*, 2002). These estimates are fairly consistent, but some diversity in estimates of the shear modulus for the lower crust is evident, with μ estimates ranging from 35 to 46 GPa. We model lower crustal μ of 30, 40, and 50 GPa, respectively (i.e., models LAY1 through LAY3), to bracket possible elasticity structures (Fig. 2). Model LAY2, with a lower crustal μ of 40 GPa, is the most consistent with seismic observations. Although a thin surface layer of very low rigidity material is likely present, particularly around the Marmara Sea, we do not model it. Incorporating this layer in our elastic models would influence displacements only within 1–2 km of the fault (Savage, 1998). GPS data from 52 sites with coseismic displacements of at least 3 mm (figure 2 of Reilinger *et al.*, 2000, Fig. 3b) are included in the inversions. The two horizontal displacement components (north and east) are used. Since (1) the mean 1σ measurement error for vertical displacements is 18 mm, as opposed to 4.3 and 5.6 mm, respectively, for the north and east components; and (2) the vertical displacements are smaller than the horizontal displacements, the horizontal displacement data would overwhelmingly control the solution if the vertical components were included.

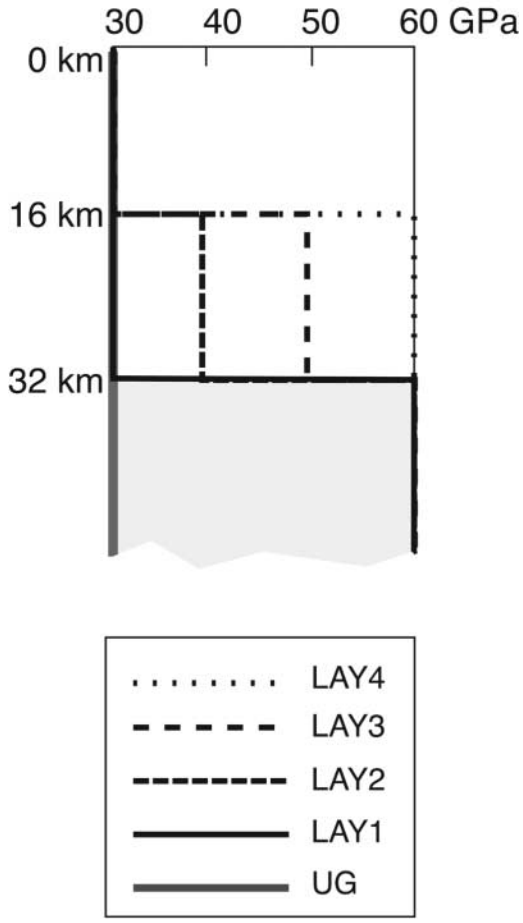

Figure 2. Models of shear modulus μ as a function of depth. UG refers to the uniform μ model, and LAY1–LAY4 are layered elastic models with successively higher values of lower crustal μ.

Results

Hypothetical Earthquake Test Models

Uniform μ *Models.* Before looking into the effects of elastic layering on recovered slip, we compared forward-modeled displacements due to slip in an elastically uniform Earth, which were obtained using the Okada, FE, and WEA methods. One of our intentions was to identify possible bias in the WEA and FE solutions relative to the Okada solution, since any bias might affect WEA and FE inversions of Izmit earthquake GPS data presented in subsequent sections of this article. Also, the only way to benchmark the WEA and FE methods to a known analytical solution is to compare their solutions for the uniform μ case with the Okada solution.

Surface displacements at the hypothetical network sites due to 3 m of slip on a 64 by 16 km fault range from 0.1 to 590 mm (Figs. 4a and 4b). The WEA-modeled east and north displacement components match the Okada solution to within 3.8 and 2.7 mm, respectively. The WRSS is 7.5, indicating a 99.99% reduction in the WRSS relative to a model

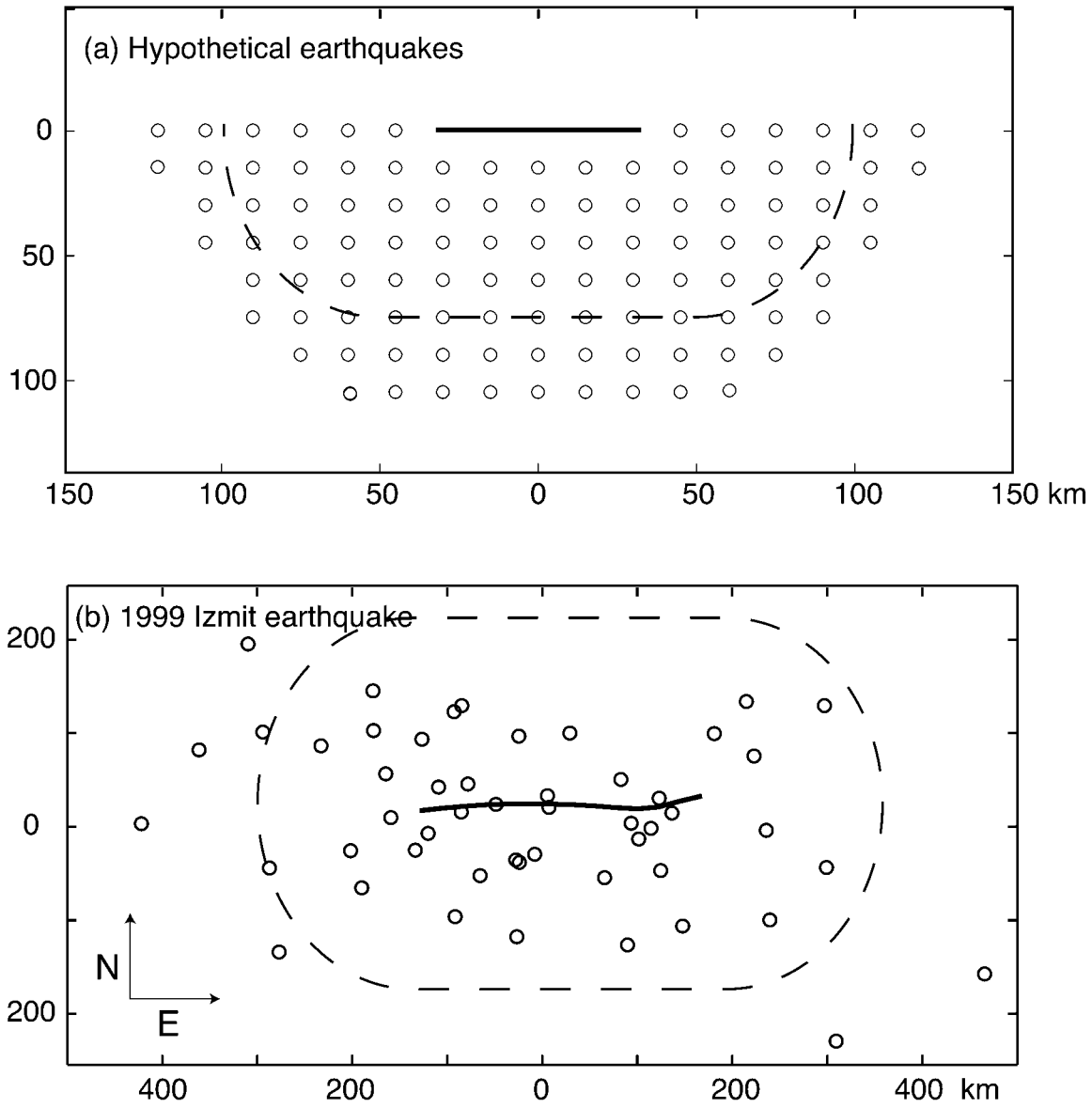

Figure 3. Distributions of GPS sites around the hypothetical strike-slip earthquake rupture (a), and the Izmit earthquake rupture (b). On (b), circles show locations of GPS sites where coseismic displacements were measured. On (a), a hypothetical network with GPS receivers spaced at 15-km intervals is shown. On (b), note that GPS receiver sites are more concentrated around the rupture and more sparse further out.

in which all surface displacements are zero. Figures 4c and 4d show contours of squared horizontal displacement residuals weighted by 1σ errors (i.e., 2 mm per degree of freedom). For the WEA solution, the largest residuals are next to the fault (Fig. 4d).

The largest residuals between the FE and Okada solutions are also adjacent to the modeled rupture (Fig. 4c), and are concentrated where the FE solution underpredicts coseismic displacements relative to the Okada solution (i.e., in the shaded area on Fig. 4a). The WRSS value for the FE solution (relative to the Okada solution) is 1785, indicating a 98.3% reduction in the WRSS relative to a model in which all surface displacements are zero.

Table 1 shows how these discrepancies would affect M_o and centroid depth (z_c) estimates for dislocations in an elastically uniform Earth. To evaluate this, we invert the forward-modeled surface displacements (described previously) for slip using the Okada method. For the Okada forward-modeled displacements due to 16-km-deep ruptures, M_o and z_c are recovered to within less than 1%. Since μ is assumed to be uniform in these inversions, the seismic potency is just M_o/μ, and this parameter is also recovered to within 1%. For

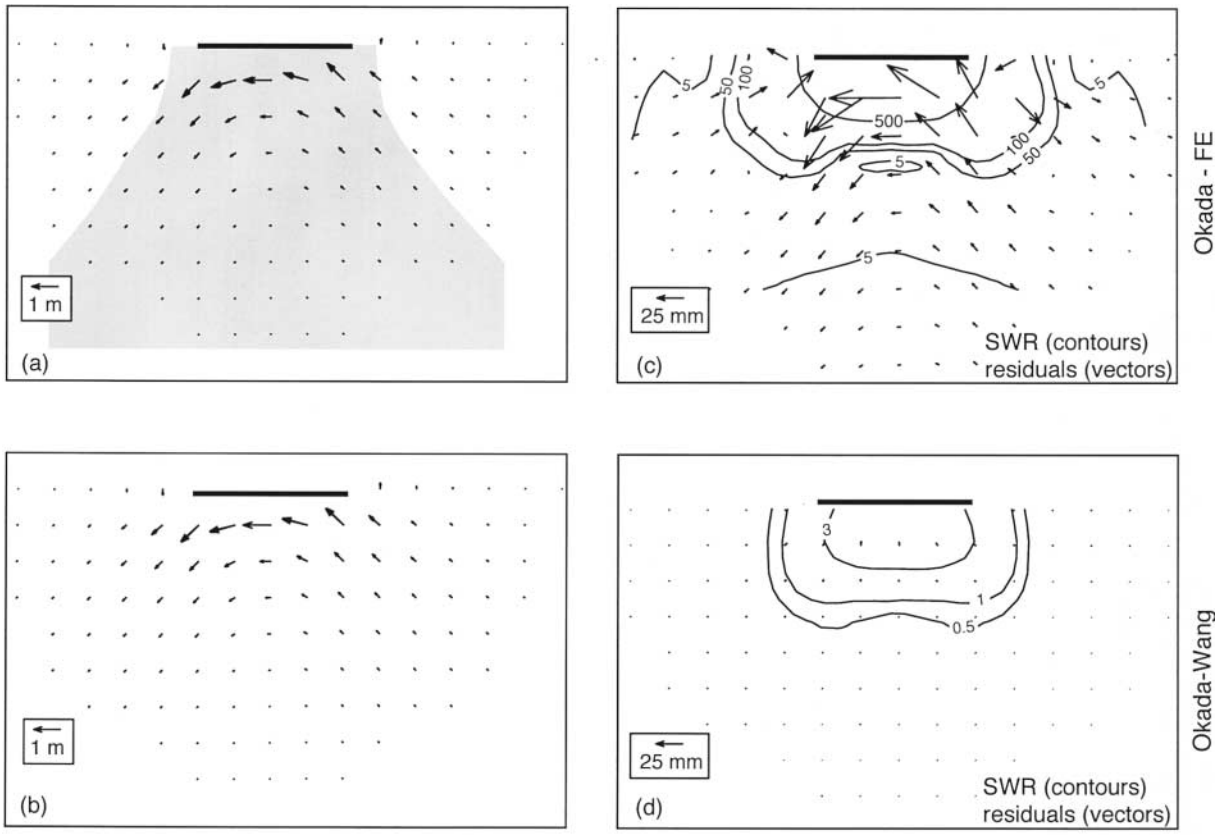

Figure 4. A comparison of forward-modeled displacements for uniform-elasticity Earth models. Results calculated using the FE and the WEA methods are compared with displacements calculated using the Okada solution. (a) and (b) show modeled displacements (indistinguishable from each other at this scale). Shading indicates where the Okada displacements are greater than the FE displacements (for the WEA, the differences in displacement amplitudes did not vary systematically with position relative to the fault). On (c) and (d), vectors show displacement residuals and contours show the spatial patterns of the squared, weighted residuals (SWR's, calculated assuming a one sigma error of 2 mm). Summing the SWR values at each (hypothetical) GPS site yields the weighted residual sum of squares (WRSS).

Table 1
Recovered Moment and Centroid Depth from Uniform-Elasticity Forward Models

Rupture Dimensions (km)	M/M(o)	z_c/z_c(o)	M(o) (N m)	Z_c(o) (km)
64 × 24	0.97 (0.99) [0.98]	1.08 (0.98) [0.98]	1.38e + 20	12
64 × 16	0.98 (0.99) [1.00]	0.98 (0.96) [1.00]	9.21e + 19	8
32 × 16	0.98 (0.99) [1.00]	0.98 (0.96) [1.00]	4.6e + 19	8

FE forward models are in plain text; WEA forward models are in parentheses; and Okada forward models are in brackets. The Okada method was used to perform these inversions.

the WEA forward-modeled displacements, M_o and z_c are recovered to within 1% and 4%, respectively. From the FE forward-modeled displacements, the Okada method recovers the M_o and z_c to within 2%.

For the deeper, 64 by 24 km rupture, recovery of z_c and M_o is only slightly poorer. z_c and M_o are recovered from the Okada and WEA forward-modeled displacements to within 1%–2%. M_o is recovered from the FE forward-modeled displacements to within 3%, but the recovered z_c for the deeper rupture is 8% too high. This is because the near-field displacements from the FE forward model are slightly smaller than displacements predicted by the Okada forward model. When the Okada **G** kernel is used to invert FE forward-modeled displacements for slip, less slip is required on the shallowest parts of the rupture to match the FE surface displacements and the deeper recovered z_c results.

Inversions of FE and WEA forward-modeled displacements for slip on the 64 by 16 km rupture, using the Okada approach, are shown on Figure 5. For the WEA displacements, slip in the top 12 km is recovered, though some smearing occurs at depth (Fig. 5b). For the FE displacements, too much slip is recovered at the ends relative to the center of the rupture (Fig. 5c). This reflects the fact that the FE

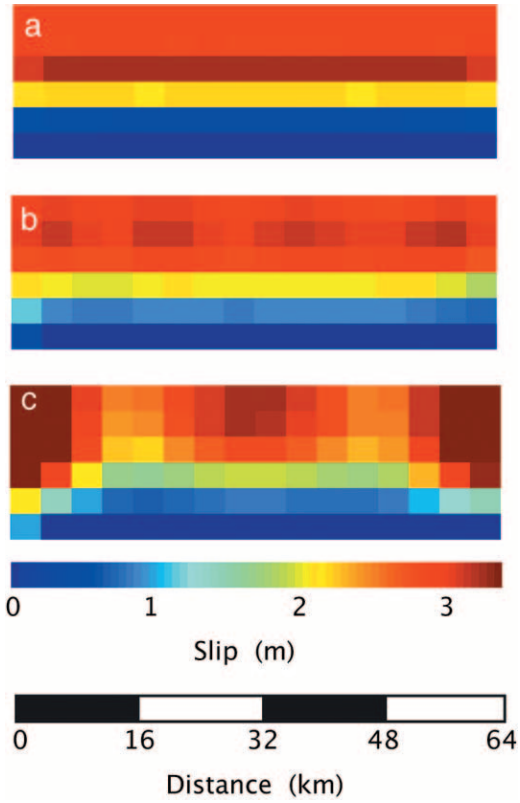

Figure 5. Slip inversions for the 64 by 16 km test model. Panel (a) shows slip recovered using the Okada method, from displacements that were forward modeled using the same method. Panels (b) and (c) show Okada inversions of displacements, which were forward-modeled using the WEA and the FE methods, respectively. The latter two forward models correspond to the surface displacements shown on Figure 4. β values are 1 km^2/m for the Okada and WEA approaches. A higher β value (10 km^2/m) was required to invert the FE forward-modeled displacements.

forward model (and hence the FE **G**) yields displacements that are too small along the rupture in the near field and too large beyond its ends, respectively (Fig. 4a).

Given the findings discussed previously, if we were to forward model displacements using the Okada method and invert them using the FE Green's functions, we would expect to underestimate z_c, particularly for deep ruptures. Hence, we could underestimate z_c when we use the FE **G** to invert Izmit earthquake GPS site displacements for fault slip. On the other hand, inversions using the WEA **G** should yield more accurate z_c results and should recover slip patterns more accurately (as suggested by Fig. 5). In the following sections of this article, we present results of inversions using both techniques, favoring those obtained from the WEA method. The FE inversions are included for comparison and discussion; this is in part because for more complex subsurface elasticity structure, the FE method is the only known technique for estimating fault slip from surface displacements.

Layered μ *Models.* In this section, we quantify the bias that results when the Okada method is used to invert coseismic surface displacements for fault slip in the real (i.e., elastically stratified) Earth. We forward model strike-slip dislocations in four different elastically-layered Earth models (see section 3.1), and then invert the displacements for slip using the Okada method. If the slip distributions are tuned so both yield similar surface displacements, the uniform μ model yields smaller M_o and shallower z_c than the layered elastic models.

For elastic model LAY1, with a μ contrast of 2 at the crust–mantle boundary, forward-modeled surface displacements attenuate more dramatically with distance from the rupture than they do in a uniform μ half-space. This has been noted (for elastic models with depth-increasing μ) by many others, for example, Rybicki (1971), Savage (1987, 1998), Pollitz (1996), and Zhao *et al.* (2004). As a result, when these displacements are inverted for M_o using the Okada method, M_o is underestimated by 16%–22%, and the recovered z_c values are about 35%–45% shallower than for the forward model (Fig. 6 and Table 2). For elastic models LAY1 through LAY4, progressive increases to the rigidity of the lower crust only slightly affect recovered z_c for the two 16-km-deep ruptures, but the recovered M_o falls progressively by another 10%–20% beyond the LAY1 recovered value (Fig. 6).

For the 24-km-deep rupture, the forward-modeled slip penetrates into the lower crust, where step increases in μ are modeled (Fig. 2). Recovered z_c deepens somewhat as crustal rigidity decreases, but is not highly sensitive to this parameter (Fig. 6). However, increases to the lower crustal μ increase the discrepancy between the forward-modeled and recovered M_o values for all three models. Changes to seismic potency are more modest than changes to M_o because some of the rupture is below a depth of 16 km, where μ is larger than in the upper crust. Discrepancies between the forward-modeled and recovered seismic potencies for these models are 12%–25%, as opposed to 16%–32% differences between forward-modeled and recovered seismic moments.

In summary, for all modeled ruptures, the μ contrast at the mantle has a more pronounced effect on recovered z_c than on recovered seismic moment. Progressive increases to lower-crustal μ have little effect on recovered z_c but affect recovered M_o as much as the mantle μ contrast (Fig. 6).

Both the FE and the WEA methods are used to forward model the displacements. As with the uniform μ models (Table 1), M_o values recovered from the FE forward models are slightly smaller than M_o values recovered from the WEA forward models. Differences in the recovered z_c values from the FE and WEA forward models are small and not systematically biased (Table 2).

Crust and Mantle Stresses. We are also interested in whether significant errors are incurred when the Okada uniform μ solution is used to calculate Coulomb stresses for earthquake probability and triggering studies. To address

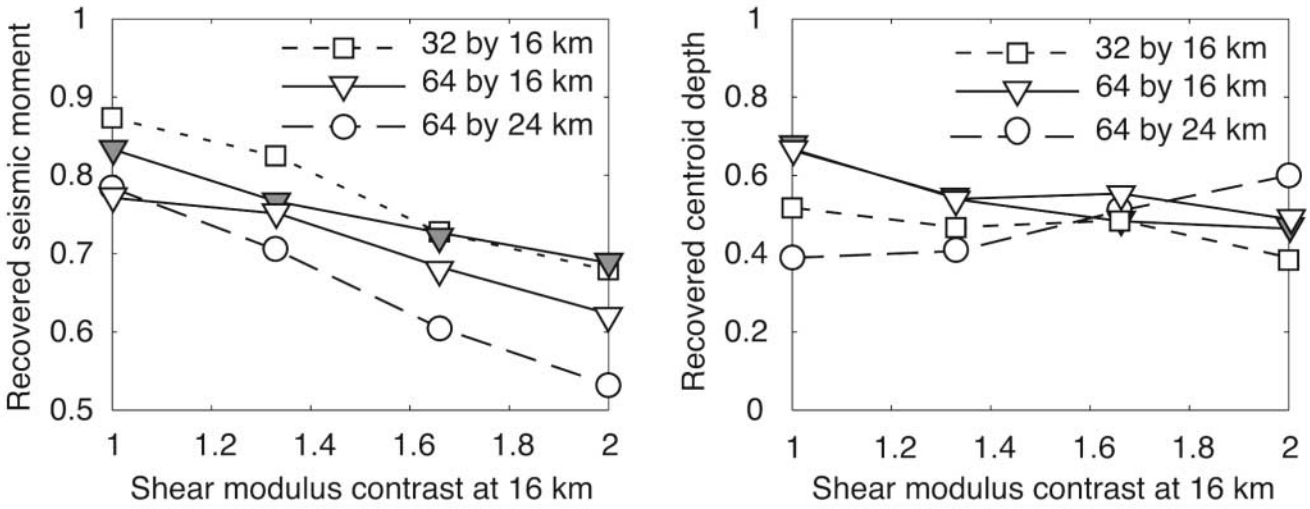

Figure 6. Recovered moment and centroid depth as a function of rigidity contrast in the midcrust, for layered elastic models of hypothetical strike-slip earthquakes. Displacements were forward modeled using layered elastic models. Uniform μ (30 GPa) was assumed in the inversions (performed using the Okada method). Open and shaded symbols show results for inversions of FE and WEA forward-modeled displacements, respectively.

Table 2
Recovered Moments and Centroid Depths: 64 by 16 km Rupture

Forward Model	UG	LAY1	LAY2	LAY3	LAY4
M_o ($\times$ 1e + 19 N m)	9.00 (9.12) [9.21]	7.2 (7.74)	7.00 (7.04)	6.19 (6.40)	5.8 (6.25)
z_c (km)	7.8 (7.56) [8.00]	5.2 (5.2)	4.3 (4.4)	4.5 (4.0)	4.1 (4.0)
WRSS	1784 (7.5) [0.3]	2664 (1854)	2566 (1754)	2780 (2549)	2711 (2002)

FE forward models are in plain text, WEA forward models are in parentheses, and Okada forward models are in brackets. The Okada method was used to perform inversions. Slip was permitted to 32 km.

this question, we calculated Coulomb stresses in the upper crust resolved onto vertical surfaces parallel to the modeled rupture (using the FE method), for the uniform μ and the LAY2 models. We find that the uniform and layered μ models give similar Coulomb stresses in the upper crust if slip is tuned to fit to the same surface displacements (Figs. 7a and 7b).

Coulomb stress (also known as the Coulomb Failure Function, or CFF) is defined as the shear stress acting on a fault surface (τ_{sh}) minus the product of the coefficient of friction (f) and the effective normal stress (σ_{eff}).

$$CFF = \tau_{sh} - f\sigma_{eff} \quad (1)$$

We assume an effective friction coefficient of 0.5, and positive normal stress is compressional. We also calculated differential stresses ($\sigma_1 - \sigma_3$) in the lower crust and upper mantle. Upper crustal stresses predicted by the uniform μ and LAY2 models differ little (Figs. 7a and 7b). In the lower crust and upper mantle, however, the uniform μ model underpredicts differential stress significantly relative to the layered Earth model (Figs. 7c–7f). In the lower crust, near-field stresses predicted by the uniform μ model are about one-third the stresses from the LAY2 model, while further from the fault, stresses predicted by the two models are approximately equal. In the upper mantle, differential stresses predicted by the uniform μ model are approximately half the magnitude of those predicted by the LAY2 model throughout the region shown on Figure 7. This is consistent with the factor-of-2 difference in mantle μ, if the modeled strain patterns are similar below the crust. We do not compare detailed patterns of modeled coseismic stress change on the rupture surface because coseismic stress change on the rupture is highly sensitive to variations in slip smoothing, and exploring this sensitivity is beyond the scope of this paper.

Izmit Earthquake

Uniform μ *Models.* Figure 8 shows slip distributions for the Izmit earthquake (assuming uniform μ), estimated using the Okada, WEA, and FE methods. These inversions yield comparable estimates of seismic moment (1.70, 1.77, and 1.86 $\times$ 10^{20} Nm, respectively). Small differences in the **G** kernel for the FE and WEA methods account for the higher

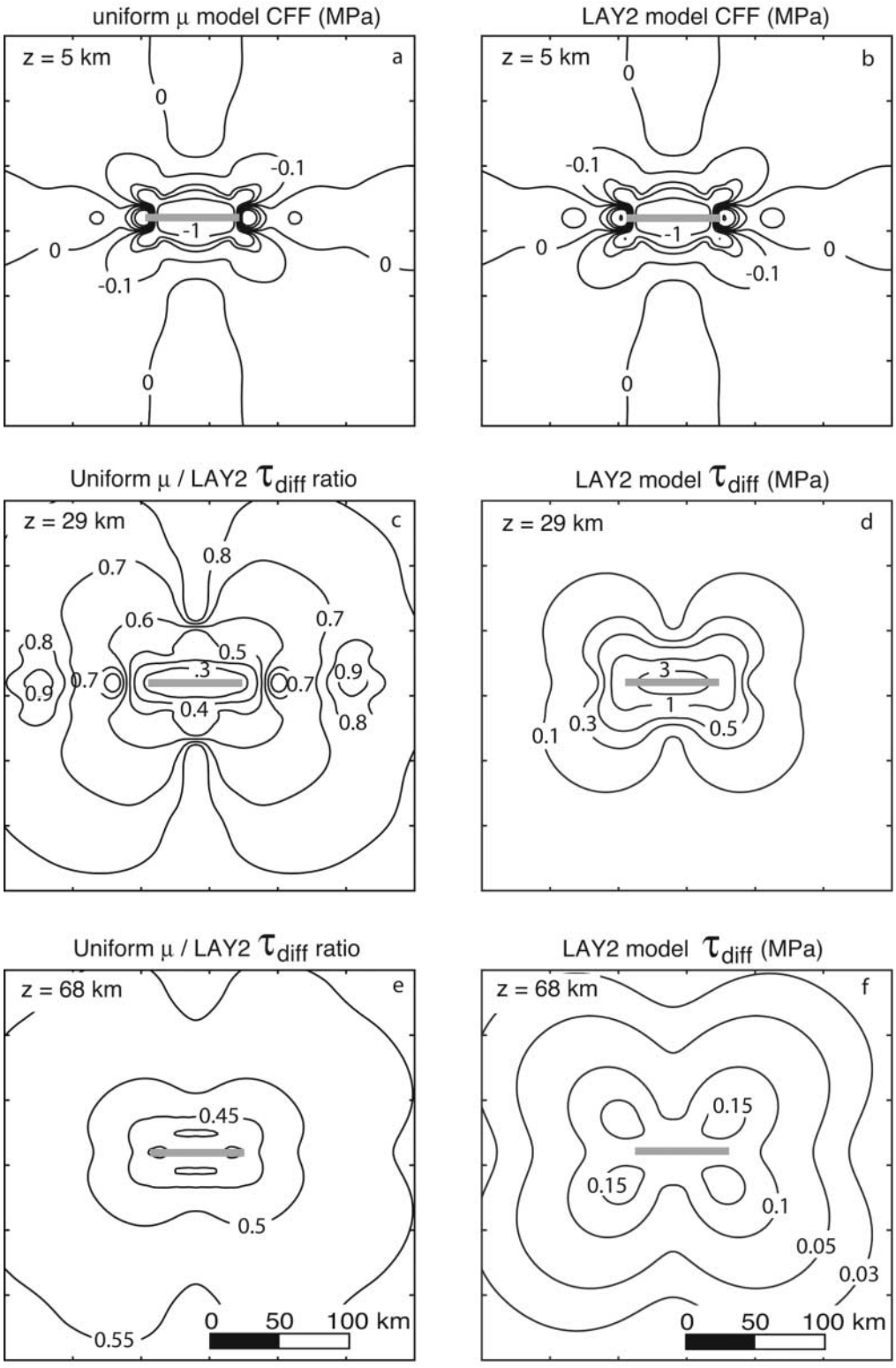

Figure 7. Forward-modeled Coulomb stresses (CFF) and differential stresses resulting from 3 m of slip on the 64 by 16 km strike-slip rupture, for the uniform μ and LAY2 elastic models. Coulomb stresses in the upper crust, calculated assuming a friction coefficient of 0.5, are similar for both models (a) and (b). In the lower crust, differential stresses from the LAY2 model are three times the values predicted by the uniform μ model, though the lower crustal μ is only 33% higher (c) and (d). Mantle stresses for the LAY2 model are about double the values for the uniform μ model, similar to the ratio of μ values (e) and (f).

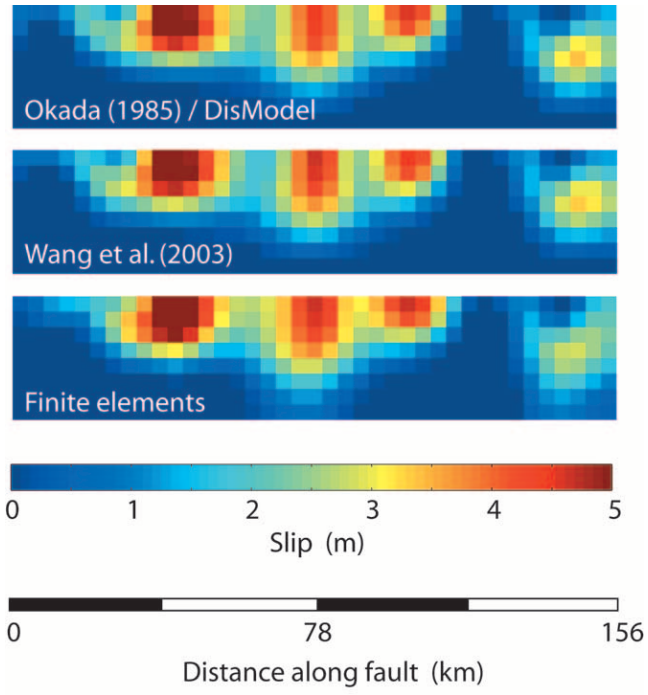

Figure 8. Izmit earthquake slip distributions for uniform μ models, calculated using the three methods discussed in the text. β is 6 km^2/m for all of the inversions.

M_o for the FE method. Centroid depths estimated from the Okada, WEA, and FE inversions are nearly identical (8.3, 8.5, and 8.5 km, respectively). Based on our findings for the test models (described previously and Table 2), we expected the FE inversion to yield a shallower z_c estimate than the WEA method. Its failure to do so may reflect the different spatial distribution of GPS sites (i.e., their concentration in the near field). In terms of general patterns, such as locations of high- and low-slip patches, the WEA and FE slip solutions are both comparable to the Okada solution (Fig. 8). Misfit to the GPS data is similar for the three uniform μ models (WRSS = 1700 to 1941).

Layered Models. Izmit earthquake slip estimates for three elastic models (LAY1–LAY3), are shown on Figure 9 and Table 3. These slip solutions show that for layered elastic models, more slip is required on and below the high-slip patches identified from Okada half-space models (e.g., Reilinger *et al.*, 2000; Feigl *et al.*, 2002; Cakir *et al.*, 2003; Fig. 8). For elastic model LAY2, the seismic moment required to optimally fit observed coseismic deformation is 2.4 $\times$ 10^{20} N m (2.5 $\times$ 10^{20} N m for the FE method), approximately 33% greater than that required by our uniform μ models. The estimated moment scales with the lower crustal rigidity, increasing from 2.1 $\times$ 10^{20} N m to 2.8 $\times$ 10^{20} N m

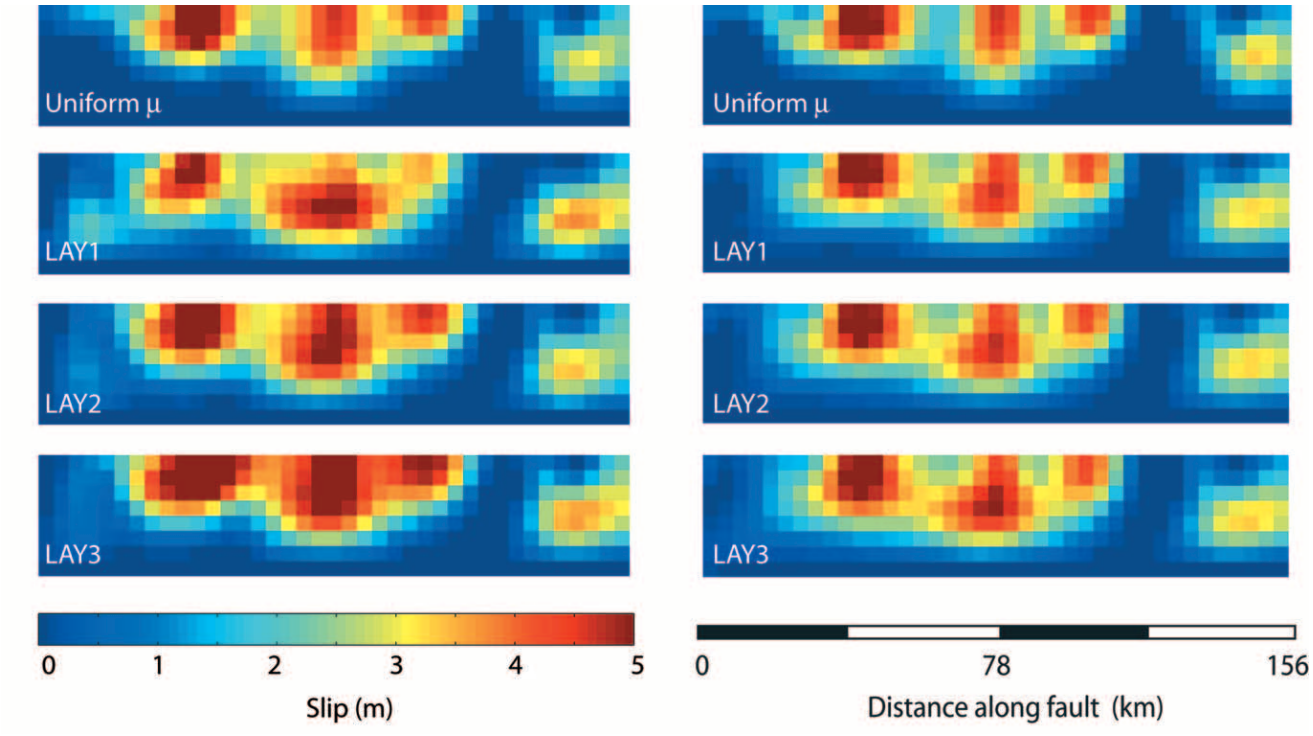

Figure 9. Izmit earthquake slip distributions for layered elastic models. Left and right columns show results for the FE and WEA approaches. Though the slip patterns are similar for all of the inversions, the layered elastic models require more slip in the midcrust. The layered elastic models (particularly LAY1 and LAY2) require slip below the upper crust on the west end of the rupture, which is not required by the uniform μ models. β is 6 km^2/m for all of the inversions.

Table 3
Recovered Moments and Centroid Depths: Izmit Earthquake

Inversion Approach	UG	LAY1	LAY2	LAY3
M_o (e + 20 N m)	1.86 (1.77) [1.70]	2.31 (2.14)	2.48 (2.43)	2.85 (2.79)
z_c (km)	8.5 (8.5) [8.3]	11.0 (10.5)	11.2 (11.8)	11.0 (13.3)
WRSS	1700 (1897) [1941]	1862 (1491)	1603 (1405)	1682 (1423)

Inversions of GPS data done using the FE, WEA, and Okada methods are in plain text, parentheses, and brackets, respectively. Slip was permitted to 32 km.

Table 4
Izmit Earthquake Moment Estimates

M_o (N m)	M_w	z_c (km)	Method	Source
Estimates assuming layered elasticity				
2.9e + 20	7.58	17	CMT	Harvard CMT webpage
2.4e + 20	7.52	13	Teleseismic	Gulen *et al.*, 2002
2.3e + 20	7.51	~10	Teleseismic	Delouis *et al.*, 2002
2.5e + 20	7.54	~8	Strong motion	Bouchon *et al.*, 2002
2.4e + 20	7.52	~8	Strong motion	Delouis *et al.*, 2002
2.2e + 20	7.50	10	GPS	This study (slip allowed to 24 km)
2.4e + 20	7.52	12	GPS	This study (slip allowed to 32 km)
Estimates made using uniform elasticity				
1.7e + 20	7.42	11	Teleseismic	Kiratzi and Louvari, 2001
1.7e + 20	7.42	6	GPS	Reilinger *et al.*, 2000
1.7–1.8e + 20	7.42–7.44	~9	GPS	Feigl *et al.*, 2002
1.7e + 20	7.42		GPS	Delouis *et al.*, 2002
1.4–1.6e + 20	7.38–7.4		InSAR	Feigl *et al.*, 2002 (ERS only)
2e + 20	7.47		InSAR	Delouis *et al.*, 2002
1.9e + 20	7.46		GPS	Cakir *et al.*, 2003*

Moment magnitudes were calculated using the method of Kanamori (1977): $M_w = 2/3 \log M_o - 6.066$. To convert to magnitudes of Hanks and Kanamori (1979), add 0.03.

z_c values with tildes were estimated from slip distributions

*Elastic parameter values were not reported in this article.

as lower crustal μ increases from 30 to 50 GPa (see Table 3 for both the WEA and FE solutions). Much of this moment increase is not associated with increased seismic potency; the seismic moment rises in part because some of the slip is below 16 km depth, where μ is higher than in the upper crust. For comparison, teleseismic moment estimates range from 2.1 to 2.4 $\times$ 10^{20} N m, strong motion estimates are 2.4 to 2.5 $\times$ 10^{20} N m, and the Harvard CMT moment (considered most accurate for very large earthquakes) is 2.9 $\times$ 10^{20} N m (see Table 4 for references). For model LAY2, z_c is estimated at 11–12 km, which is more consistent with seismic estimates of 10 to 17 km (Table 4) than our uniform μ z_c estimate of 8.5 km.

A Tikhonov plot (WRSS versus roughness) for elastic model LAY2 (WEA method) is shown on Figure 10. Finite-difference estimates of the curvature of this plot suggest that β should be between 2 and 20 km^2/m. We have chosen to use β = 6 km^2/m for the Izmit slip inversions. Z_c and M_o estimates are not highly sensitive to β within the range β = 1–20, so our choice of β does not affect our conclusions. For example, the moment and z_c estimates from an Okada inversion of displacements due to slip on a 64 by 16 km dislocation in the LAY2 model vary from 6.9 to 7.1 $\times$ 10^{19} N m and from 4.4 to 4.6 km as β is varied from 1 to 11.

One parameter we wish to resolve as well as possible is the maximum depth of coseismic slip during the Izmit earthquake. To investigate this, we invert the surface displacements for slip, allowing slip down to maximum depths of 16, 20, 24, 28, and 32 km. If the fit to surface displacements degrades for the shallow ruptures, a minimum limit may be placed on the maximum depth of coseismic rupture (z_m). Figures 11 and 12 show how misfit correlates with z_m for the uniform μ model and for models LAY1 through LAY3. For uniform μ models, increasing z_m has little to no effect on misfit, or on estimates of centroid depth or seismic moment (Fig. 11). This means that the rupture may extend to just 16 km, or even less. For the layered elastic models, however, the WRSS increases significantly if the rupture is restricted to the top 20 km of the crust (Fig. 12). Allowing slip deeper than 24 km improves the model fit to the GPS data only modestly, though moment and centroid depth estimates continue to increase. Hence, conservative estimates for M_o and z_c (2.2 $\times$ 10^{20} N m and 10 km, respectively) are obtained from models in which slip is not permitted below 24 km.

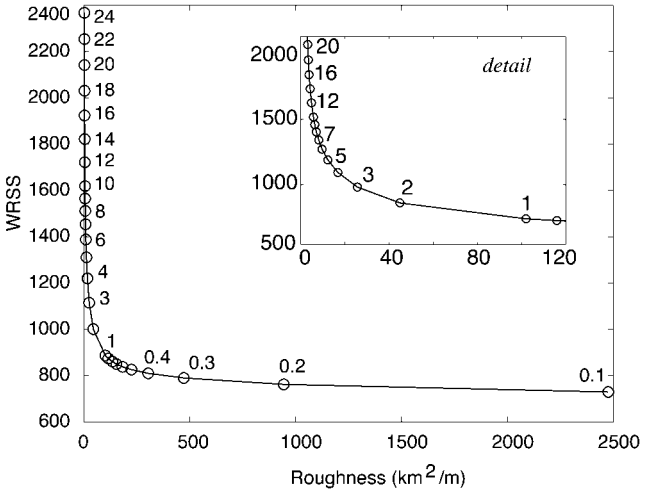

Figure 10. Tikhonov plot showing WRSS as a function of smoothing parameter for Izmit earthquake slip inversions (LAY2 elastic model). Values of β (in km^2/m) are shown on the plot. The optimal β value is where the curvature is at a maximum (e.g., Hansen, 1998). The maximum curvature values (from a finite-difference estimate) occur for β values between 2 and 20. We choose $\beta = 6$ km^2/m.

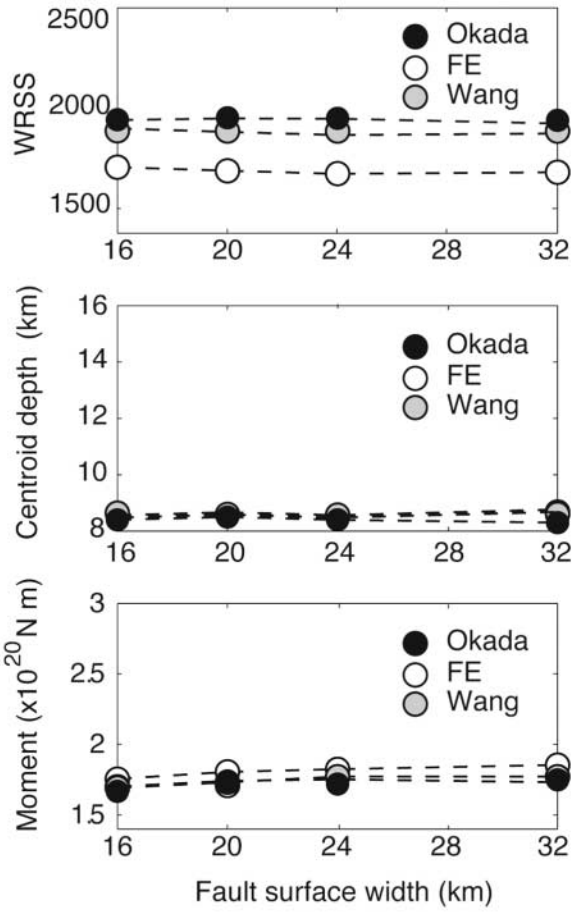

Figure 11. Weighted residual sum of squares (WRSS), centroid depth, and moment from uniform μ Izmit models, as a function of maximum permitted rupture depth. Even though fewer fault tiles are used to represent the fault in the shallower rupture models, fit is not degraded by limiting the rupture to the uppermost 16 km of the crust.

Spatial patterns of the residuals between GPS data and displacements from the best LAY2 models with $z_m = 16$ km and 32 km indicate that allowing slip to extend into the mid- to lower crust improves the fit to displacement data at most sites and reduces the WRSS by a factor of 2 (Fig. 12). Hence, the reduction in WRSS is not due to a large improvement in model performance at one or two sites. To investigate how much of this effect is due to downward smearing of slip by the smoothing operator, we also looked at the correlation between WRSS and depth of rupture for models with $\beta = 1$. These models give results similar to those on Figure 12, except that the absolute values of WRSS are smaller.

Figures 13 and 14 compare crust and mantle coseismic stress changes from the uniform μ and LAY2 models of the Izmit earthquake. In the upper crust, Coulomb stresses resolved onto vertical, east–west oriented surfaces are shown. In the lower crust and upper mantle, differential stresses (σ_1–σ_3) are shown. Upper crustal stresses predicted by the two models differ little, which suggests that for stress triggering studies incorporating coseismic stress changes, the uniform μ assumption would be adequate in the area shown. In the lower crust and upper mantle, however, the uniform μ model underpredicts differential stress significantly relative to the layered Earth model. In the lower crust, near-field stresses are too low by a factor of 2 to 3, while further from the fault, stresses predicted by the two models are approximately equal. In the upper mantle, differential stresses predicted by the uniform μ model are approximately half the magnitude of those predicted by the LAY2 model throughout the region shown on Figure 14. Given the factor-of-2 difference in mantle μ values for the two models, this indicates similar patterns and magnitudes of elastic mantle strain.

Discussion

Slip Inversions

Elastic layering significantly affects surface deformation due to faulting. As a result, z_c and seismic potency recovered from inversions of GPS data may be underestimated significantly if the Earth is modeled as a uniform elastic half-space, regardless of the assumed μ value. Furthermore, if a low (i.e., upper crustal) value of μ is assumed, as is common practice, the recovered M_o will be too low. As expected from the Savage (1987) solution for the effect of layering on toroidal mode (2D) deformation due to a dislocation in the upper crust, we find that the layering effect is smallest if the rupture depth is much less than the depth to the first transi-

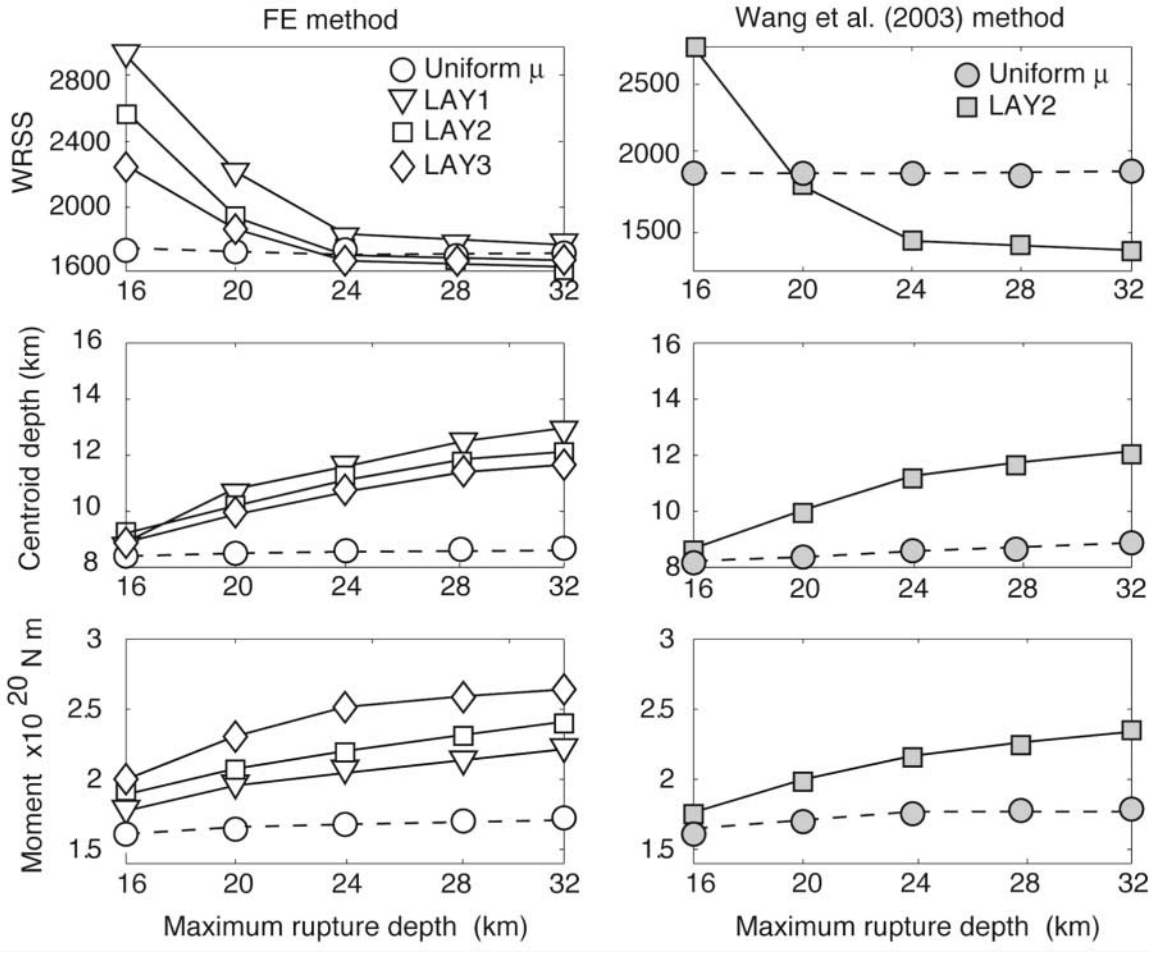

Figure 12. Weighted residual sum of squares (WRSS), centroid depth, and moment from layered μ Izmit models, as a function of maximum permitted rupture depth. The WRSS increases sharply when the maximum rupture depth is restricted to less than 20 km. Increasing the maximum rupture depth beyond 24 km does not improve the fit to GPS data.

tion in μ, and if the increase in μ is modest. For large strike-slip earthquakes, recovery of centroid depths is affected more by the presence of a high μ contrast at the Moho, whereas recovery of M_o is influenced more by μ contrasts within the crust.

Inversions of GPS displacement data from the 1999 Izmit earthquake in which a uniform μ of 30 GPa is assumed underestimate both moment and centroid depth by about 30% relative to inversions in which the more realistic LAY2 elastic structure is modeled. These results are approximately comparable to those shown on Figure 6 for our hypothetical earthquake models. The most analogous case is the 64 by 16 km rupture in the LAY2 elastic model, for which the Okada model underestimates moment and z_c by 25% and 45%, respectively. Given the effect of restricting the maximum slip depth on model misfit (Fig. 12), we conclude that the Izmit earthquake ruptured to a depth of at least 20 km.

We did not explicitly investigate how varying the spatial distributions of observation points would affect our main conclusions for the hypothetical rupture models. For a particular GPS network, the effect of elastic layering on observed deformation should depend on the relative contributions of poloidal and toroidal deformation at site locations and on distances from observation sites to the rupture. Layering affects the toroidal and poloidal deformation components differently. In semianalytical elastic solutions (e.g., Wang *et al.*, 2003, and other solution techniques listed therein) the two, uncoupled components are separated and displacement solutions propagated through the layered model differently. This means that, theoretically, inverting deformation associated with each mode will yield a different slip solution, unless the correct elastic structure is used to generate the data kernel **G**. On the other hand, since measurement errors are smallest for the horizontal deformation, and since large strike-slip earthquakes yield mostly toroidal surface deformation, varying station distributions should have little effect on potential biases in estimated z_c and moment.

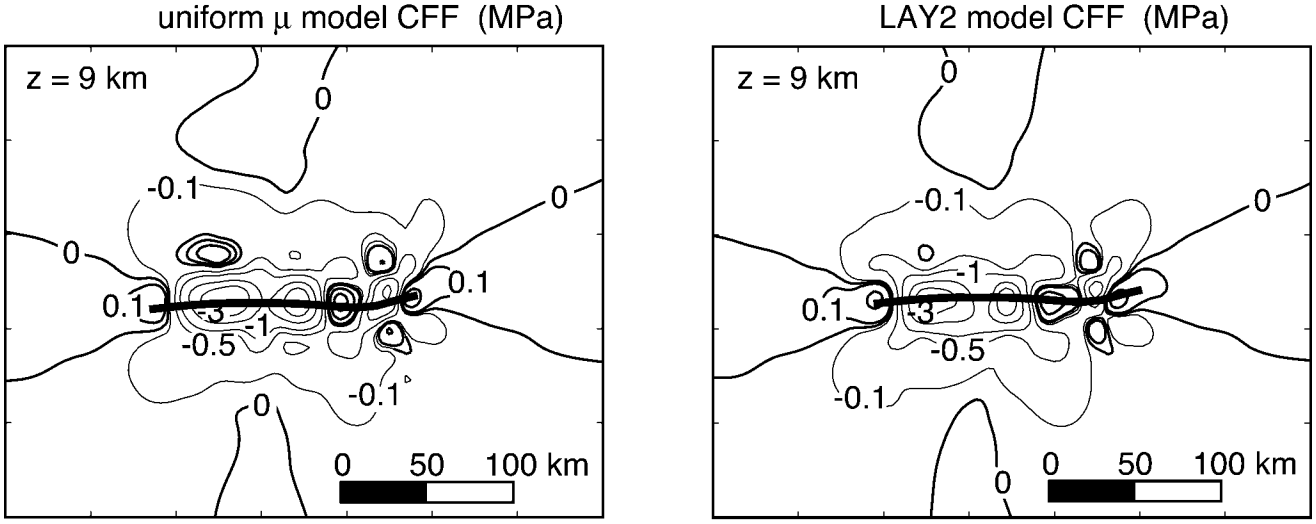

Figure 13. Forward-modeled Coulomb stresses for uniform μ and LAY2 elastic models of the Izmit earthquake. Slip distributions from the inversions shown on Figure 8 are modeled. Coulomb stresses in the upper crust, calculated assuming a friction coefficient of 0.5, are similar for both models.

Reconciling Seismic and Geodetic Slip Distributions

Feigl (2002) has compiled a list of source parameter estimates from large earthquakes around the world to illustrate differences between geodetic and seismic (CMT) moment estimates. He lists several reasons for discrepancies between seismic and geodetic moment estimates, including different measurement time intervals (GPS measurements generally span longer intervals and may include some postseismic deformation), and different assumed values of μ. He shows that, in general, seismic moments are larger than seismic moments, principally because of the longer measurement time interval. This effect has been demonstrated for the Izmit earthquake by Cakir *et al.* (2003) and for the Northridge earthquake by Dreger (1997), who attribute it to aseismic afterslip and large aftershocks, respectively. However, of the large ($M \geq 7$) strike-slip earthquakes for which Feigl (2002) presents both seismic and geodetic moment estimates, these estimates are not systematically different, though scatter is significant (see Feigl [2002], Table 1, and Fig. 3).

Recent analyses of geodetic slip from the Landers and Hector Mine, California, earthquakes (Austin and Miller, 2002; Jonsson *et al.*, 2002; Kaverina *et al.*, 2002; Simons *et al.*, 2002) conclude that seismic moments are either slightly less than or equal to the CMT moments for these events. For other earthquakes, the geodetic and seismic moment estimates differ more. Most of the seismic moment estimates for the Izmit earthquake are about 40% smaller than the CMT moment and about 25% smaller than other seismological estimates (Table 4). For the 2002 Denali earthquake, the most recent GPS and inSAR moment estimates are 9% to 10% lower than the CMT moment (S. Hreinsdöttir *et al.*, unpublished manuscript, 2005; Wright *et al.*, 2004). For all of these events, excluding layered elasticity from the inversions is skewing the geodetic M_o estimates toward smaller values, though by varying degrees. As we have demonstrated for the Izmit earthquake (Hearn *et al.*, 2002), incorporating layered elasticity should bring geodetic and seismic moment estimates for large strike-slip earthquakes into better alignment.

Implications for Earthquake Triggering and Fault Interaction Studies

We compare broader patterns of coseismic stress changes in the crust and mantle surrounding the hypothetical and real earthquake ruptures, and find the effects of layering to be similar for the hypothetical rupture and the Izmit earthquake (Figs. 7 and 13). Coulomb stresses in the upper crust (on vertical surfaces parallel to the main fault, at a depth of 5 to 9 km) appear to be insensitive to elastic layering, as long as the coseismic slip is tuned to optimally fit surface deformation data. Differences in both the horizontal shear and tensile CFF components are modest, which suggests that this conclusion should hold for vertical strike-slip faults, regardless of their orientation. We note that differences in CFF of the order of 0.01 MPa are present within about 50 km of the Izmit rupture, and note that in the extreme near field and near the base of the upper crust, the differences could be greater. However, given the sensitivity of near-field CFF estimates to other parameters, which are characterized with some uncertainty (e.g., elastic structure, fault geometry, and slip patterns, including the extent of slip smoothing), we do not regard these differences as significant. We also note that the spatial patterns of regions with positive CFF are insensitive to layered elasticity, and differences in CFF estimates in the far field are small, even in a relative sense. Still, as

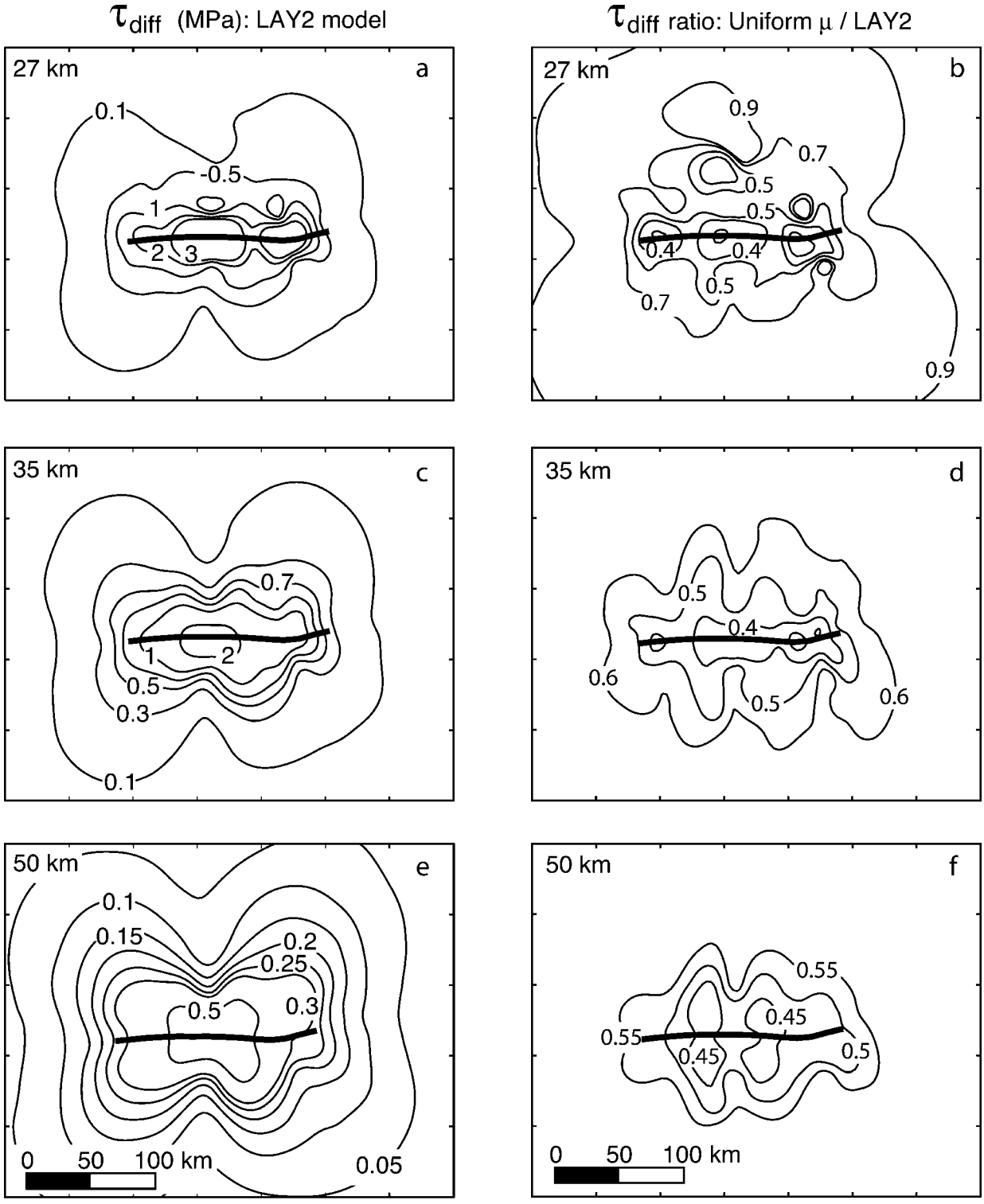

Figure 14. Forward-modeled differential stresses for uniform μ and LAY2 elastic models of the Izmit earthquake. (a), (c), and (e) show differential stresses in MPa. (b), (d), and (f) show the ratio of differential stresses for the uniform μ model (μ = 30 GPa) relative to results from the LAY2 model. In the lower crust, differential stresses from the LAY2 model are about 2.5 times the values predicted by the uniform μ model, though the lower crustal μ is only 33% higher (a) and (b). With increasing depth in the mantle, stresses for the LAY2 model approach values of about double the values for the uniform μ model, reflecting the ratio of μ values for the two models.

more precise characterization of fault slip and geometry, and elastic structure become commonplace, the effect of layered elasticity on near-field CFF should be revisited.

Zhao *et al.* (2004) obtain larger differences in upper crustal stresses than we do, for a smaller strike-slip earthquake (0.5 m slip on a 25-km-long, 10-km-deep rupture). There are two reasons for this. First, in their layered models they model a μ contrast in the upper crust at 5 km depth, and use a more exaggerated increase in μ (actually Young's modulus) with depth, particularly in their model C. Also, Zhao *et al.* impose the same slip in all three of their elastic models. We model more slip in our layered elastic models to match GPS surface displacements, and this tends to bring modeled crustal stresses for the two models toward agreement.

Differential stresses in the lower crust are significantly higher in the near field for layered elastic models, though further from the fault, the stresses approach those predicted by the uniform μ models. Since μ in the lower crust is greater than 30 GPa for our layered elastic model LAY2, the elevated stresses relative to the uniform μ models reflect higher strain near the fault, but lower strains further from the fault. Near-field stress patterns in the midcrust are likely complicated, and we did not model them with enough resolution to comment on the details of how these stresses achieve their deviation from the Okada solution deep in the crust. Hence, for earthquakes nucleating at the base of the seismogenic zone and within about one fault length of the rupture, we cannot determine whether the Okada approach is sufficiently accurate for estimating stresses at the hypocenter.

Coseismic strain and stress concentrations in excess of what uniform μ models predict could drive faster postseismic surface deformation in the near field. The resulting surface deformation rates could mimic the postseismic response of a less viscous lower crust, or even (because of the relative concentration of stress and high strain rates in the near field) a nonlinearly viscoelastic lower crust. However, many recent postseismic deformation models incorporate depth-dependent lithosphere elasticity (e.g., Pollitz and Sacks, 2002; Freed and Bürgmann, 2004) and implicitly account for this effect. Deeper in the mantle, the ratio of modeled stresses becomes more uniform throughout the modeled region, and approaches the ratio of the modeled mantle μ values for the layered and uniform models (i.e., two). This suggests that in the mantle, layered and uniform μ models produce similar patterns of strain. Similar patterns and rates of early postseismic relaxation should result if the modeled mantle Maxwell times (η/μ) are the same.

Conclusion

Incorporating realistic depth dependence of μ increases our estimates of z_c and seismic potency relative to Okada (uniform μ) models. For some earthquakes, particularly in regions with a significant contrast in μ in the middle crust, incorporating depth-dependent μ may double estimates of the centroid depth, and (to a lesser degree) increase estimates of maximum slip depth. Estimated M_o is also greater (by up to 40%) for models incorporating depth-dependent μ than for Okada half-space models, in which an upper crustal values of μ is assumed. Given these findings, we can explain the persistent difference between geodetic and seismological estimates of M_o for large strike-slip earthquakes, in cases where the GPS coseismic displacement data capture little postseismic deformation. This discrepancy arises because most seismological slip inversions account for elastic layering while most geodetic slip inversions do not.

Estimates of coseismic stress in the upper crust are not significantly altered by incorporating depth-dependent elasticity in our models (except in the extreme near field), as long as slip at depth in the layered model is tuned to match surface displacements. However, modeled coseismic stress changes in the lower crust and upper mantle increase by up to a factor of 3. In the lower crust, this difference is restricted to the near field. Deeper in the mantle, the difference in differential stress is more widespread and approaches the ratio of mantle μ values for the layered and uniform models. We conclude that models of postseismic viscoelastic relaxation or afterslip following large strike-slip earthquakes should incorporate depth-dependent elasticity. Uniform half-space elastic models are adequate (except in the near field) for calculating CFF in the upper crust for studies of earthquake triggering following large strike-slip earthquakes.

Acknowledgments

We would like to thank Fred Pollitz and an anonymous reviewer for their helpful comments on this article. This research was supported by the Southern California Earthquake Center (SCEC) and by E. Hearn's NSERC Discovery Grant. SCEC is funded by NSF Cooperative Agreement EAR-0106924 and USGS Cooperative Agreement 02HQAG0008. The SCEC contribution number for this article is 850.

References

Austin, K. E., and M. Miller (2002). The coseismic displacement fields for the 1992 Landers and 1999 Hector Mine earthquakes in California, from regional GPS observations, *Bull. Seis. Soc. Am.* **92,** 1365–1376.

Bouchon, M., M. N. Toksoz, H. Karabulut, M. P. Bouin, M. Dieterich, M. Aktar, and M. Edie (2002). Space and time evolution of rupture and faulting during the 1999 Izmit (Turkey) earthquake, *Bull. Seism. Soc. Am.* **92,** 256–266.

Bürgmann, R., S. Ergintav, P. Segall, E. Hearn, S. McClusky, R. E. Reilinger, H. Woith, and J. Zschau (2002). Time-dependent distributed afterslip on and deep below the Izmit earthquake rupture, *Bull. Seism. Soc. Am.* **92,** 126–137.

Cakir, Z., J.-B. de Chabalier, R. Armijo, B. Meyer, A. Barke, and G. Pelzer (2003). Coseismic and early postseismic slip from the 1999 Izmit earthquake (Turkey), from SAR interferometry and tectonic field observations, *Geophys. J. Int.* **155,** 93–110.

Chinnery, M. A. (1961). The deformation of the ground around surface faults, *Bull. Seism. Soc. Am.* **51,** 355–372.

Delouis, B., D. Giardini, P. Lundgren, and J. Salichon (2002). Joint inversion of InSAR, GPS, teleseismic, and strong-motion data for the spatial and temporal distribution of earthquake slip: application to the 1999 Izmit mainshock, *Bull. Seism. Soc. Am.* **92,** 278–299.

Dreger, D. (1997). The large aftershocks of the Northridge earthquake and their relationship to mainshock slip and fault zone complexity, *Bull. Seism. Soc. Am.* **87,** 1259–1266.

Du, Y., A. Aydin, and P. Segall (1998). Comparison of various inversion techniques as applied to the determination of a geophysical deformation model for the 1983 Borah Creek earthquake, *Bull. Seism. Soc. Am.* **82,** 1840–1866.

Feigl, K. (2002). Estimating earthquake source parameters from geodetic measurements, in *International Handbook of Earthquake Engineering and Seismology, Part A*, W. Lee, H. Kanamori, P. Jennings, and C. Kisslinger (Editors), Academic, New York.

Feigl, K. L., F. Sarti, H. Vadon, S. McClusky, S. Ergintav, P. Durand, R. Bürgmann, A. Rigo, D. Massonet, and R. Reilinger (2002). Estimating slip distribution for the Izmit mainshock from coseismic GPS, RADARSAT, ERS-1, and SPOT measurements, *Bull. Seism. Soc. Am.* **92,** 138–160.

Fialko, Y. (2004). Probing the mechanical properties of seismically active crust with space geodesy: study of the co-seismic deformation due to the 1992 M_w 7.3 Landers (southern California) earthquake, *J. Geophys. Res.* **109,** B08401, doi 10.1029/2003JB002756.

Freed, A., and R. Bürgmann (2004). Evidence of power-law flow in the Mojave upper mantle, *Nature*, **430,** 548–551.

Gulen, L., A. Pinar, D. Kalafat, N. Ozel, G. Horasan, M. Yilmazer, and A. Isikara (2002). Surface fault breaks, aftershock distribution, and rupture process of the 17 August 1999 Izmit, Turkey, earthquake, *Bull. Seism. Soc. Am.* **92,** 230–244.

Hanks, T., and H. Kanamori (1979). A moment magnitude scale, *J. Geophys. Res.* **84,** 2348–2350.

Hansen, P. C. (1998). *Rank-Deficient and Discrete Ill-Posed Problems: Numerical Aspects of Linear Inversion*, SIAM, Philadelphia.

Harris, R., and P. Segall (1987). Detection of a locked zone at depth on the Parkfield, California section of the San Andreas fault, *J. Geophys. Res.* **92,** 7945–7962.

Hearn, E. H., R. Bürgmann, and R. E. Reilinger (2002). Dynamics of Izmit earthquake postseismic deformation and loading of the Duzce earthquake hypocenter, *Bull. Seism. Soc. Am.* **92,** 172–193.

Jonsson, S., H. Zebker, P. Segall, and F. Amelung (2002). Fault slip distribution of the 1999 M_w 7.1 Hector Mine earthquake, California, estimated from satellite radar and GPS measurements, *Bull. Seism. Soc. Am.* **92,** 1377–1389.

Kanamori, H. (1977). The energy release in great earthquakes, *J. Geophys. Res.* **82,** 2981–2987.

Karabulut, H., M. Bouin, M. Bouchon, M. Dietrich, C. Cornou, and M. Aktar (2002). The seismicity in the eastern Marmara Sea after the 17 August 1999 Izmit earthquake, *Bull. Seism. Soc. Am.* **92,** 387–393.

Karahan, A. E., H. Berckhemer, and B. Baier (2001). Crustal structure at the western end of the North Anatolian fault zone from deep seismic sounding, *Annali de Geofisica* **44,** 49–68.

Kaverina, A., D. Dreger, and E. Price (2002). The combined inversion of seismic and geodetic data for the source process of the 16 October 1999 M_w 7.1 Hector Mine, California, earthquake, *Bull. Seism. Soc. Am.* **92,** 1266–1280.

Kiratzi, A., and E. Louvari (2001). Source parameters of the Izmit-Bolu 1999 (Turkey) earthquake sequences from teleseismic data, *Annali de Geofisica* **44,** 33–47.

Melosh, H. J., and A. Raefsky (1981). A simple and efficient method for introducing faults into finite element computations, *Bull. Seism. Soc. Am.* **71,** 1391–1400.

Okada, Y. (1995). Surface deformation due to shear and tensile faults in a half-space, *Bull. Seism. Soc. Am.* **75,** 1135–1154.

Pollitz, F. F. (1996). Coseismic deformation from earthquake faulting on a layered spherical Earth, *Geophys. J. Int.* **125,** 1–14.

Pollitz, F. F., and I. S. Sacks (2002). Stress triggering of the 1999 Hector Mine earthquake by transient deformation following the 1992 Landers earthquake, *Bull. Seism. Soc. Am.* **92,** 1487–1496.

Price, E. J., and R. Bürgmann (2002). Interactions between the Landers and Hector Mine, California earthquakes from space geodesy, boundary element modeling, and time-dependent friction, *Bull. Seism. Soc. Am.* **92,** 1450–1469.

Reilinger, R., S. Ergintav, R. Bürgmann, S. McCluskey, O. Lenk, A. Barka, O. Gurkan, E. Hearn, K. L. Feigl, R. Cakmak, B. Aktug, H. Ozener, and M. N. Toksoz (2000). Coseismic and postseismic fault slip for the 17 August 1999, M = 7.5, Izmit, Turkey Earthquake, *Science* **289,** 1519–1524.

Rybicki, K. (1971). The elastic residual field of a very long strike-slip fault in the presence of a discontinuity, *Bull. Seism. Soc. Am.* **61,** 79–92.

Saucier, F., and E. D. Humphreys (1993). Horizontal crustal deformation in Southern California from joint models of geologic and very long baseline interferometry measurements, in *Contributions of Space Geodesy to Geodynamics*, D. E. Smith and D. L. Turcotte (Editors), *AGU Geodyn. Ser.* **23,** Washington D.C., 139–176.

Savage, J. C. (1987). Effect of crustal layering upon dislocation modeling, *J. Geophys. Res.* **92,** 10,595–10,600.

Savage, J. C. (1998). Displacement field for an edge dislocation in a layered half space, *J. Geophys. Res.* **103,** 2439–2446.

Simons, M., Y. Fialko, and L. Rivera (2002). Co-seismic static deformation from the 1999 M_w 7.1 Hector Mine, California, earthquake, as inferred from InSAR and GPS observations, *Bull. Seism. Soc. Am.* **92,** 1390–1402.

Stark, P. B., and R. L. Parker (1995). Bounded variable least-squares: an algorithm and applications, *Comput. Statist.* **10,** 129–141.

Wang, R., F. L. Martin, and F. Roth (2003). Computation of deformation induced by earthquakes in a multi-layered elastic crust—FORTRAN programs EDGRN/EDCMP, *Comp. Geosci.* **29,** 195–207.

Wells, D. L., and K. J. Coppersmith (1994). New empirical relationships among magnitude, rupture length, rupture width, rupture area, and surface displacement, *Bull. Seism. Soc. Am.* **84,** 974–1002.

Wright, T. J., Z. Lu, and C. Wicks (2004). Constraining the slip distribution and fault geometry of the M_w 7.9, 3 November 2002, Denali fault earthquake with interoferometric synthetic aperture radar and global positioning system data, *Bull. Seism. Soc. Am.* **94,** no. 6B, S175–S189.

Zhao, S., R. Müller, Y. Takahashi, and Y. Kaneda (2004). 3-D finite-element modelling of deformation and stress associated with faulting: effect of inhomogeneous crustal structures, *Geophys. J. Int.* **157,** 629–644.

Department of Earth and Ocean Sciences
University of British Columbia
Vancouver, British Columbia, Canada
ehearn@eos.ubc.ca
(E.H.H.)

Department of Earth and Planetary Sciences
University of California at Berkeley
Berkeley, California
Burgmann@seismo.berkeley.edu
(R.B.)

Manuscript received 16 August 2004.